Wide Bandwidth and Low Driving Voltage Vented CMUTs for Airborne Applications

Bo Ma, *Graduate Student Member, IEEE*, Kamyar Firouzi, *Member, IEEE*,
Kevin Brenner, and Butrus T. Khuri-Yakub, *Life Fellow, IEEE*

***Abstract*— This paper presents a novel method to increase the bandwidth (BW) of airborne capacitive micromachined ultrasonic transducers (CMUTs). This method introduces a gaseous squeeze film as a damping mechanism, which induces a stiffening effect that lowers the pull-in voltage and improves the sensitivity. The optimal behavior of this stiffening effect versus the damping mechanism can be controlled by creating optimized fluidic trenches of various heights within the gap. The fractional BW can be controlled from 0.89% to 8.1% by adjusting the trench height while lowering the pull-in voltage to less than 54 V at the gap height of 1.0 μm. To achieve the largest sensitivity and lowest pull-in voltage at a given BW, we have developed a multi-parameter optimization method to adjust all combinations of design parameters. A novel multiple hard-mask process flow has been developed to enable fabrication of CMUTs with different cavity and trench heights on the same wafer. These devices provided an equivalent noise pressure level of 4.77 μPa/$\sqrt{}$Hz with 6.24-kHz BW for 7.6-μm deep fluidic trenches and 4.88 μPa/$\sqrt{}$Hz with 7.48-kHz BW for 14.3-μm deep fluidic trenches. This demonstration of the wide-BW CMUTs with high sensitivity and low pull-in voltage makes them applicable to medical and thermoacoustic imaging, nondestructive testing, and ultrasonic flow metering.**

***Index Terms*— Capacitive micromachined ultrasonic transducers (CMUTs), low driving voltage, multi-parameter optimization, multiple hard-mask microfabrication, squeeze film, wide bandwidth (BW).**

I. Introduction

CAPACITIVE micromachined ultrasonic transducers (CMUTs) have emerged as an alternative to piezoelectric transducers, offering advantages such as wide bandwidth (BW), ease of fabricating large arrays, and easy integration with supporting electronic circuits. As such, CMUTs are ideal for applications in medical imaging, therapeutics, chemical sensing, and air-coupled ultrasound. In airborne applications, such as thermoacoustic root imaging, both high sensitivity and wide BW are desired. Sensitivity relates to the ability to detect small signals while BW relates to resolution. However, the BW of conventional vacuum CMUTs is not wide enough in such applications [1]. As such, attempts have been made to widen the BW. For example, Olcum *et al*. [2] defined a gain–BW product and investigated the conditions to maximize this performance. Zhang *et al*. [3] used a thin plate and increased the fill factor to broaden the BW of a CMUT array. Unlugedik *et al*. [4], [5] have employed the stiffening effect created by the atmospheric pressure to improve BW. However, both of these methods are limited by physics and the fabrication process. Kupnik *et al*. [6] and Bayram *et al*. [7] designed a CMUT array with different sizes connecting in parallel to get a larger BW at the expense of gain and transducer size. Apte *et al*. [8], [9] explored a method to broaden the BW by introducing a gaseous squeeze film as a damping mechanism. However, introducing a squeeze film will result in a significant decrease in sensitivity and dramatic increase in the pull-in voltage. To obtain the best balance, we have developed a multi-parameter optimization method to adjust the design parameters to achieve the best sensitivity and lowest pull-in voltage at a given BW [10].

In this paper, to widen the CMUT BW while obtaining low minimum detectable pressure (MDP), we present a novel method. This method is based on the squeeze film damping and can maintain a constant sensitivity–BW product as the BW is tuned. Furthermore, it guarantees a very low acoustic loss through vented vias. The method makes full use of the damping effect of the squeeze film, in which the BW and resonant frequency can be controlled by adjusting the damping. The gap height can be lowered to the order of 1.0 μm, decreasing the driving voltage significantly. We have designed and optimized fluidic trenches for adjusting the squeeze film damping to control the BW by merely changing the trench height. Based on the optimal design, the fractional bandwidth (FBW) can be easily managed while reducing the pull-in voltage. Finally, the designed CMUTs with different trench heights have all been fabricated on a single wafer based on our multiple hard-mask microfabrication processes. The impedance and vibration displacement measurements confirm the feasibility of the theory and give a very low MDP.

II. Equivalent Circuit Modeling

Typically, a CMUT is a variable capacitor coupled to an acoustic medium. The capacitor consists of a flexible plate, an insulation layer, and a fixed substrate, as shown in Fig. 1. A gap is formed between the flexible top plate and the fixed substrate. Both the plate and substrate are made electrically conductive to form a capacitor across the gap. The insulating layer is used to prevent the two electrodes from electrically

Manuscript received April 5, 2019; accepted July 7, 2019. Date of publication July 11, 2019; date of current version October 24, 2019. This work was supported by the Advanced Research Projects Agency-Energy (ARPA-E) through the ROOTS Program under Grant DE-AR0000825. *(Corresponding author: Bo Ma.)*

The authors are with the Department of Electrical Engineering, Stanford University, Stanford, CA 94305 USA (e-mail: mabo@stanford.edu).

Digital Object Identifier 10.1109/TUFFC.2019.2928170

0885-3010 © 2019 IEEE. Personal use is permitted, but republication/redistribution requires IEEE permission.
See http://www.ieee.org/publications_standards/publications/rights/index.html for more information.

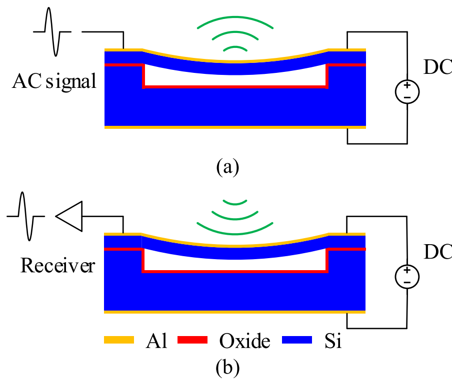

Fig. 1. Schematic of a conventional CMUT. (a) Transmitter and (b) receiver.

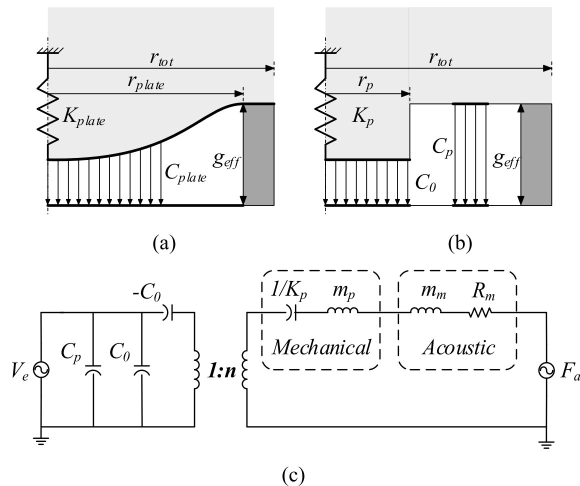

Fig. 2. Equivalent piston model of CMUT and the small-signal equivalent circuit. (a) Cross section of CMUT. (b) Cross section of the equivalent piston. (c) Small-signal equivalent circuit.

shorting. In typical operation, the CMUT is biased with a direct current (dc) voltage, which generates an electrostatic force that deflects the flexible plate toward the substrate and forms an active capacitor that functions as an electromechanical transformer. For a transmitter, an alternating current (ac) signal modulates the electrostatic force and harmonically moves the flexible plate, hence generating an ultrasound wave into the surrounding medium. For a receiver, an ultrasound wave impinges on the flexible plate and causes the vibration of the plate, which in turn changes the active capacitance and generates an electric current. This current is converted into a voltage output through a receiver circuit.

A. Small-Signal Equivalent Circuit

A CMUT can be modeled as an equivalent lumped parameter piston transducer [11], [12], as shown in Fig. 2. The piston is held over an effective electrostatic gap by a spring. The flexible plate can be modeled with an equivalent spring K_p and a mass m_p corresponding to the plate resonant frequency. The electric field within the gap generates an electrostatic force that moves the plate, and thus, converts the electrical energy to the mechanical one. The capacitance includes two parts: one is the active capacitance C_0 corresponding to the electromechanical transformer; the other is the parasitic capacitance C_p. The acoustic medium presents an impedance to the transducer. Based on Mason's theory [13], under a small ac voltage or acoustic pressure, the piston model can be further transformed into a small-signal equivalent circuit [14], [15], as shown in Fig. 2(c). In the equivalent circuit model, the mechanical impedance consisting of the equivalent mass and spring is represented by an inductor and a capacitor, respectively. The acoustic impedance comprising of a damping load R_m and a mass load m_m is described as the medium resistance and inductance.

For a small dc bias voltage, the piston reaches an equilibrium displacement where the electrostatic force balances the spring restoring force. Due to the nonlinear nature of electrostatic force as a function of the plate displacement, pull-in occurs when the electrostatic force gradient overcomes the gradient of the mechanical restoring force; thus, the piston collapses onto the substrate for a bias voltage larger than the pull-in voltage V_{PI}. The maximum equilibrium displacement is one-third of the effective gap height. The pull-in voltage is given by [16]

$$V_{\mathrm{PI}} = \sqrt{\frac{8K_p g_{\mathrm{eff}}^3}{27\varepsilon_0 A_p}} \quad (1)$$

where K_p is the stiffness of the equivalent piston, g_{eff} is the effective gap height, and A_p is the equivalent actuation area. Therefore, the pull-in voltage strongly depends on the effective gap height and the actuation area at a set resonant frequency. The electrostatic force between the CMUT's electrodes does not vary linearly with the CMUT plate's displacement. However, the restoring spring force of the CMUT plate, which is balanced with the electrostatic force varies linearly with its displacement; therefore, as the plate moves toward the substrate, the nonlinear electrostatic force increases significantly and makes it appear as if the CMUT plate is becoming soft. This is the so-called electrostatic spring softening effect, which is converted to $-C_0$ in the equivalent circuit by moving it to the electrical side.

B. Sensitivity and Bandwidth Calculation

According to the equivalent circuit model, the transfer function of a CMUT can be derived in the transmit mode by setting the acoustic source F_a zero. Acoustic pressure can be calculated by dividing the acoustic force [the voltage across R_m in Fig. 2(c)] by the plate area A_{plate}. The maximum transmit sensitivity occurs at the resonant frequency and is given by [15]

$$S_{\mathrm{Tx,max}} = n/A_{\mathrm{plate}} \quad (2)$$

where n is the electromechanical transformer ratio, which represents the energy conversion efficiency. At a given dc bias, n can be calculated as follows:

$$n = E_0 C_0. \quad (3)$$

Here, E_0 is the strength of the electric field at the given dc bias. The maximum transmit sensitivity only depends on the transformer ratio when the plate is fixed by a specific application. Therefore, reducing the gap height remains the only means of improving the transmit sensitivity.

Similarly, by setting the electrical source V_e zero, we can derive the transfer function in the receive mode. The maximum receive sensitivity is given by

$$S_{\mathrm{Rx,max}} = nA_{\mathrm{plate}}/R_m. \tag{4}$$

$S_{\mathrm{Rx,max}}$ not only depends on the transformer ratio but also the medium damping. However, the medium is determined by the target application. Hence, increasing the transformer ratio is the only viable way to improve the receive sensitivity.

It is easy to verify that the BW and FBW are

$$\mathrm{BW} = \frac{R_m}{m_{\mathrm{tot}}}$$
$$\mathrm{FBW} = \frac{R_m}{\sqrt{m_{\mathrm{tot}}K_{\mathrm{tot}}}} \tag{5}$$

where the total mass m_{tot} includes the medium and equivalent piston mass, while the total spring stiffness K_{tot} consists of the piston stiffness and the electrostatic spring softening effect.

To achieve a wider BW, we could design a CMUT with a thinner plate that yields a smaller mass. However, a smaller mass means a softer spring for the same resonant frequency and a smaller electromechanical transformer ratio at the same percentage of dc bias. Therefore, a wider BW results in lower sensitivity. For a very thin plate, geometrical nonlinearity also needs to be considered [17]. Adding other damping sources may become an alternative way to broaden the BW without significantly sacrificing its sensitivity. The damping sources could be squeeze film damping or mechanical damping. Squeeze film damping is widely used in the microphone industry [18], [19] and can be easily introduced by venting the CMUT cavity. Therefore, in this paper, we have introduced squeeze film damping and optimize the fluidic trenches to improve the BW.

III. Gaseous Squeeze Film Damping

As micro-electromechanical systems (MEMS) devices decrease in size, the effects of surface forces become more significant. As a result, the motion of a MEMS structure can be significantly affected by the surrounding gas or fluid. As the gas film is commonly on the order of micrometers, the squeeze film will dominate the dynamic behavior of microstructures [20]. Generally, the squeeze film would degrade the quality factor of MEMS devices. Therefore, others have focused on decreasing the squeeze film by perforating microstructures in the past [21]–[23]. However, here we could take advantage of the damping effect of the squeeze film to broaden the BW in CMUTs. As shown in Fig. 3(a), the squeeze film is introduced by venting through the CMUT cavity.

A. Lumped Parameter Model

The behavior of squeeze film in CMUTs is generally governed by the classical Reynolds equation, which is characterized by the Reynolds number. In most MEMS devices, the Reynolds number is small enough to make the inertia effect of fluid negligible. In CMUTs, the relative movement in the lateral direction can also be neglected. Hence, the Reynolds equation is given by [18], [22]

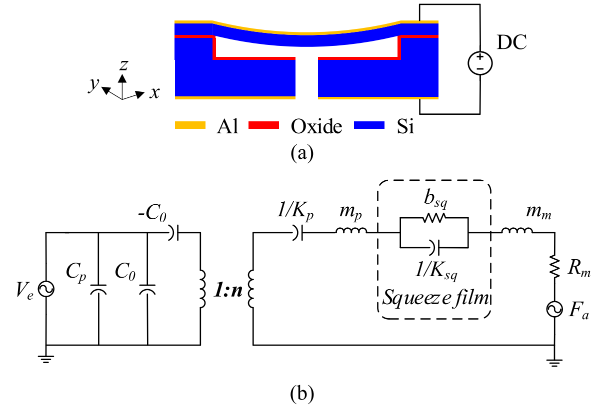

Fig. 3. Schematic of a vented CMUT and the equivalent circuit model. (a) Schematic and (b) equivalent circuit with added squeeze film.

$$\frac{\partial}{\partial x}\left(\rho_f \frac{g^3}{\mu}\frac{\partial P}{\partial x}\right) + \frac{\partial}{\partial y}\left(\rho_f \frac{g^3}{\mu}\frac{\partial P}{\partial y}\right) = 12\frac{\partial (g\rho_f)}{\partial t} \tag{6}$$

where ρ_f is the density of the fluid film, P is the pressure generated by the squeeze film, and μ is the coefficient of viscosity of the fluid. In the equivalent piston model, the gap g is not a function of the position, and viscosity is independent of the piston. Therefore, after normalization, (6) can be further simplified as

$$\frac{\partial^2}{\partial \hat{x}^2}\hat{P}^2 + \frac{\partial^2}{\partial \hat{y}^2}\hat{P}^2 = 2\sigma\frac{\partial (\hat{g}\hat{P})}{\partial \hat{t}} \tag{7}$$

where $\hat{P} = P/P_a$, $\hat{x} = x/l$, $\hat{y} = y/l$, and $\hat{g} = g/g_{\mathrm{eff}}$. P_a is the static ambient pressure inside the CMUT cavity, l is the typical length of the plate, and g_{eff} is the equivalent gap height. The dimensionless constant σ is known as the squeeze number. In the case of a circular CMUT, the squeeze number is given by

$$\sigma = \frac{12\mu\omega r_0^2}{P_a g^2} \tag{8}$$

where r_0 is the plate radius. Solving the normalized Reynolds equation and taking the first-order approximation, the ratio of the squeeze force $\hat{F}_{\mathrm{sq}}(s)$ (Laplace transform) to the displacement function $\hat{z}(s)$ (Laplace transform) for a circular plate can be obtained as [24]

$$\frac{\hat{F}_{\mathrm{sq}}(s)}{\hat{z}(s)} = \frac{b_{\mathrm{sq}}s}{\left(1+\frac{s}{\omega_c}\right)}$$
$$b_{\mathrm{sq}} = \frac{4.45\mu r_0^4}{g^3}$$
$$\omega_c = \frac{g^2 P_a}{2.07\mu r_0^2}. \tag{9}$$

Therefore, according to the Laplace transform of the spring-mass-damper system, the squeeze film can be modeled as a lumped spring-damping mechanical system after neglecting the mass of gas molecules, which consists of a damper b_{sq} in

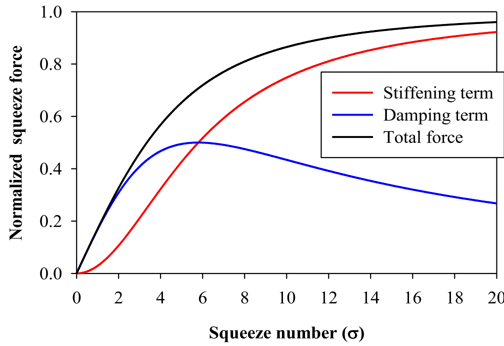

Fig. 4. Contribution of the damping and stiffening component of the squeeze force. The damping and stiffening terms present the real and imaginary parts of the squeeze force, respectively.

series with a spring K_{sq}. However, it can be converted into a resistor b_{sq} in parallel with a capacitor $1/K_{sq}$ in the equivalent circuit. The modified equivalent circuit with the added squeeze film term is shown in Fig. 3(b).

By replacing R_m with $R_m + R_{sq}$ in (5), the BW can be rewritten as

$$\mathrm{FBW} = \frac{R_m + R_{sq}}{\sqrt{m_{tot} K_{tot}}} \tag{10}$$

where R_{sq} is the resistance derived from the squeeze film, and the total spring constant K_{tot} consists of the stiffness of the equivalent piston, electrostatic spring softening effect, and squeeze film stiffening effect. Therefore, we can control the BW by designing and optimizing the squeeze film.

B. Damping and Stiffening Effect

For any particular frequency ω, we can substitute $s = j\omega$ in (9). For low frequencies $\omega << \omega_c$, the squeeze film acts as a viscous damper with damping constant b_{sq}. For high frequencies, the squeeze film acts as a spring in which the stiffness can be written as

$$K_{sq} = \frac{2.15 P_a r_0^2}{g}. \tag{11}$$

The squeeze number determines the proportion of the damping and stiffening component and can be expressed as $\sigma = 5.8\omega/\omega_c$ with the cutoff frequency ω_c. The higher the squeeze number, the harder it is for the fluid to move in and out of the film gap. Hence, the squeeze force mostly contributes to the stiffening of the squeeze number $\sigma >> 5.8$. For a lower squeeze number, $\sigma < 5.8$, the fluid can easily move in and out of the film gap. Hence, the squeeze force mostly contributes to damping. The contribution of the damping and stiffening effect of squeeze force is shown in Fig. 4. As mentioned before, we could tune the damping and stiffening effect in the squeeze film to control the BW and sensitivity of CMUTs.

IV. Design and Optimization

A. Multi-Parameter Optimization Method

Introduction of the squeeze film damping increases the BW at the cost of significantly reducing the sensitivity as well as increasing the driving voltage. Optimizing these parameters to achieve an optimal performance can be challenging. A single-parameter optimization or naive sweeping method cannot find the best tradeoffs between the sensitivity, BW, and driving voltage. Because all the parameters have coupled effects on the CMUT's performance, the optimal behavior cannot be reached merely by tuning a specific parameter, while keeping the other parameters fixed. A multi-parameter optimization method provides a suitable means of resolving this issue [25].

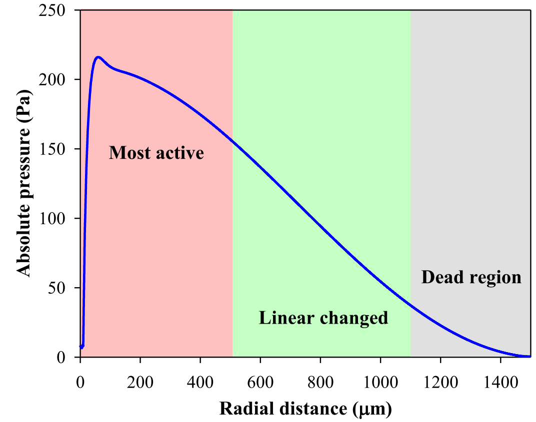

Fig. 5. Absolute squeeze pressure on the substrate of the vented CMUTs with one via at the center.

We have developed a multi-parameter optimization method for improving CMUT sensitivity and BW [10]. In the multi-parameter optimization, the objective is to get the maximum sound pressure under the constraint of the given minimum BW. The maximum output sensitivity can be achieved by looking for an optimal parameter combination of the control variables such as plate radius, gap height, as well as via radius and distribution. The pull-in voltage and the resonant frequency can be considered as the other constraints.

B. Design and Optimization of Fluidic Trenches

The absolute pressure on the substrate for a vented CMUT with one via at the center is shown in Fig. 5. The distribution of the absolute pressure on the substrate is nonuniform. The pressure on the radius line of the plate shows that the substrate can be divided into three regions: the central region, which is the most active, the middle region, and the edge region. The most active region contributes to the most significant vibration, thus resulting in a higher pressure on the substrate. Also, this region provides the most significant output pressure. In the linear region, the absolute pressure on the substrate behaves linearly in relationship with the radius and has a decreasing trend. The so-called dead region has nearly no contribution to the vibration, as well as the output pressure and pull-in voltage, but contributes to the most parasitic capacitance. According to this distribution map, the optimization of fluidic trenches can also be divided into three types of structures to make the most effective use of the area of the substrate electrode.

One common way to control the squeeze film is to perforate the plate. Some researchers have previously analyzed the impact of the squeeze film on perforated plates [20]–[22]. However, perforating either the plate or the substrate to vent

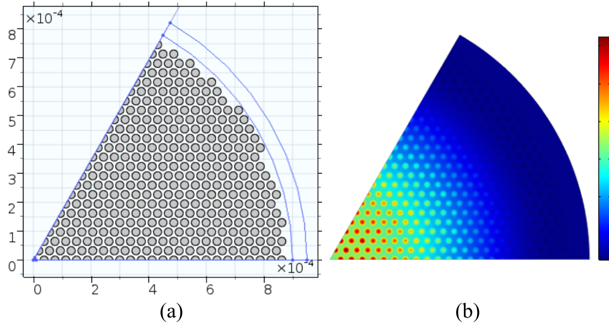

Fig. 6. Micropillar fluidic array. (a) Distribution and (b) absolute pressure on the surface of the substrate electrodes.

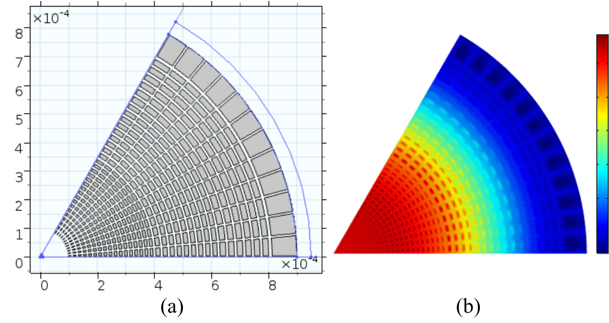

Fig. 7. Fan-shaped fluidic trenches. (a) Distribution and (b) absolute pressure on the surface of the substrate electrodes.

the cavities will introduce other issues such as limited transmit and receive sensitivity, high pull-in voltage, introducing other resonant modes by mounting, and significant acoustic loss through the perforating holes [8]. In the following, we propose three methods.

1) Micropillar Array: The gap height should be as low as possible to decrease the pull-in voltage. In this case, the stiffening effect will dominate the behavior of the squeeze film, which causes the resonant frequency to increase significantly. On the contrary, increasing the gap height to adjust the damping effect of the squeeze film will increase the pull-in voltage significantly. As such, a circle array of cylindric micropillars is an efficient way to tune the stiffening and damping effect with the same distribution of the perforated holes [21], as shown in Fig. 6. Micropillar array trenches can make the gap height lower than 1 μm, but keep the resonant frequency as designed with the substrate electrode ratio of 51%. The absolute pressure can consequently be lowered to one-tenth of that of without fluidic trenches in the substrate.

2) Fan-Shaped Trenches: As shown in Fig. 6(b), the absolute pressure on the micropillar array surface is nonuniform. The pressure drops significantly with the increase of the radius. This means that the electrode area has not been effectively used. Therefore, a geometry with an increasing electrode area is needed. Fig. 7 shows a fan-shaped structure in which the area of the electrode can be adjusted nearly linearly with the radius. The fan-shaped fluidic trenches significantly improve the uniformity of the absolute pressure on the substrate at the linear region. The area ratio of the electrode can be increased to 88%, which in turn reduces the pull-in voltage further.

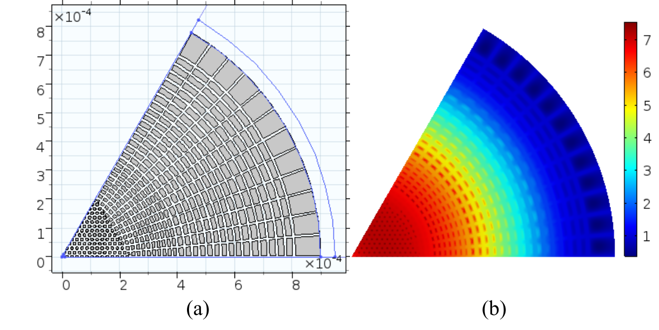

Fig. 8. Hybrid fluidic trenches. (a) Distribution and (b) absolute pressure on the surface of the substrate electrodes.

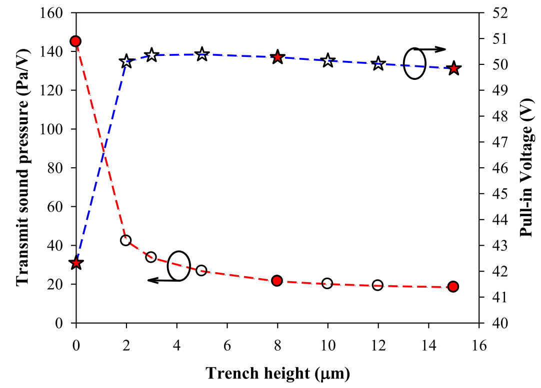

Fig. 9. Transmit sensitivity and pull-in voltage versus trench height.

3) Hybrid Fluidic Trenches: The hybrid fluidic trenches are formed by combining the micropillar array and fan-shaped fluidic trenches, as shown in Fig. 8. These hybrid fluidic trenches can reduce the squeeze film most effectively while maintaining a large electrode area. The area ratio of the electrode reaches 86%, which decreases 10% of the pull-in voltage further. Fig. 8 also shows that the absolute pressure on the surface of the hybrid fluidic trenches distributes much more uniformly.

C. Performance Optimization

After optimizing the geometry and distribution of the fluidic trenches, the trench height is used as a unique control parameter to tune the damping effect, and thus, control the BW of the CMUT. However, the pull-in voltage does not change much with the trench height because the area of the substrate electrode stays nearly fixed, as shown in Fig. 9. Finally, the pull-in voltage has been lowered to less than 50 V, which is 3.2 times lower than the previous design [9]. Low pull-in voltage makes these wide-BW CMUTs a feasible choice for medical imaging, as well as smart wearable/implantable medical devices, which requires low power consumption. Fig. 10 shows the receive sensitivity and the BW as a function of the trench height. By increasing trench height, the transmit and receive sensitivity reduces gradually. Accordingly, the BW would increase significantly. The FBW can be improved from 0.74% to 7.4% at the cost of compromising some sensitivity. Sensitivity and BW are a tradeoff parameter pair.

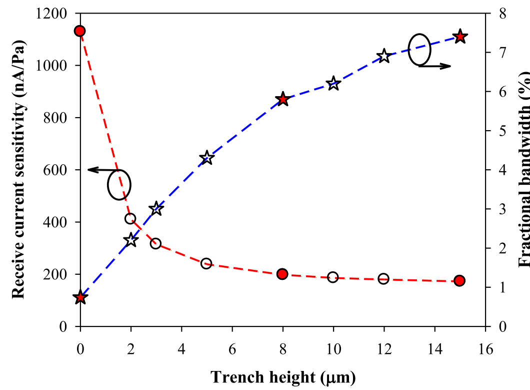

Fig. 10. Receive sensitivity and FBW versus trench height.

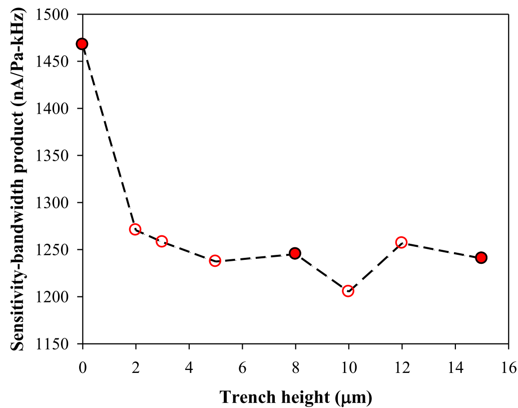

Fig. 11. Sensitivity–BW product versus trench height.

Increasing the BW drops the sensitivity. However, in our designs, by adjusting the trench height to control the BW, the sensitivity–BW product is kept nearly constant, as shown in Fig. 11.

V. Fabrication

We have developed a novel multiple hard-mask microfabrication process, in which CMUTs with different cavity and trench heights can be fabricated on a single wafer. This is typically not possible as the cavity and trenches for the entire wafer are defined by a single etch. As such, all various CMUT designs, all within the desired BW of 0.74% to 7.4%, can be built on a single wafer, which significantly reduces the fabrication cost. The developed process is based on the wafer-bonding technology [26], which provides the advantage of low residual stress and uniform plate thickness. Fig. 12 shows the flow of the multiple hard-mask processes.

First, a 1.0-μm-deep cavity for vented CMUTs and 0.5-μm-high stoppers are etched by deep reactive ion etching (DRIE), which gives good control over the gap height [as shown in Fig. 12(a)]. Stoppers are used to prevent stiction between the substrate and the plate after its release. Next, a thick oxide layer (SiO_2) of 1.2-μm thickness is thermally grown [Fig. 12(b)]. Then, one layer of 300-nm polysilicon [as shown in Fig. 12(c)], as the mask for etching

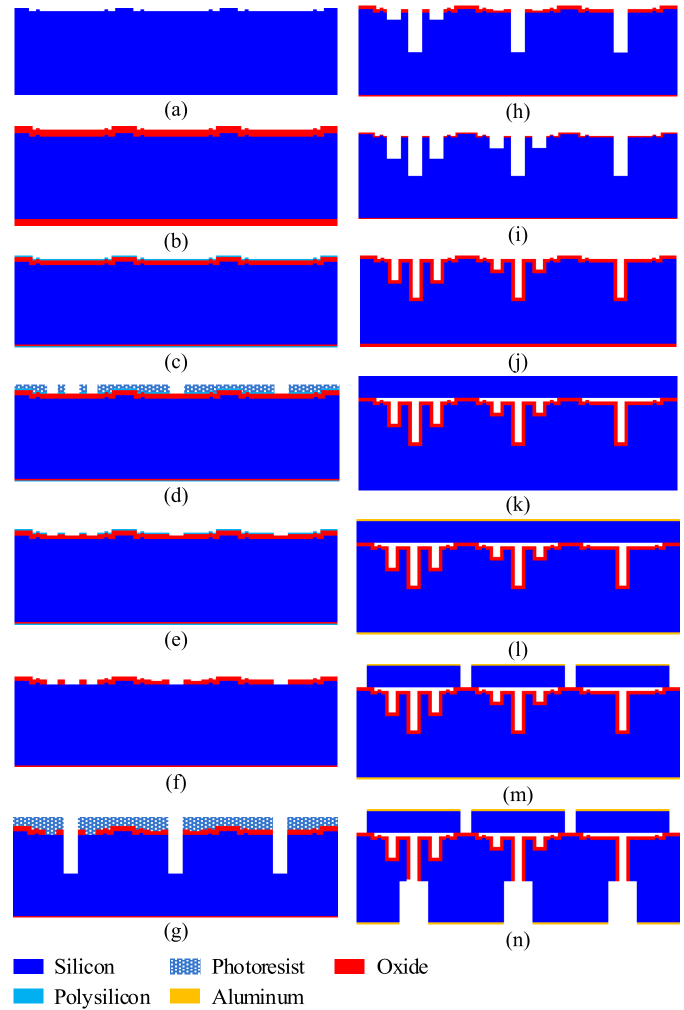

Fig. 12. Fabrication flow of the multiple hard-mask process. (a) DRIE for cavities and stoppers. (b) Thermal oxidation. (c) LPCVD for the poly layer. (d) Lithography for the 1st oxide mask. (e) Etch for the 1st oxide mask. (f) Pattern for the 2nd oxide mask. (g) Deep etch for front via. (h) Etch for 15-μm-deep trenches. (i) Etch for 8-μm-deep trenches. (j) Thermal oxidation. (k) Direct wafer bonding. (l) Sputter aluminum. (m) Pattern for the flexible plate. (n) Deep etch for backside via.

oxide, is deposited by low-pressure chemical vapor deposition (LPCVD). The poly layer [as shown in Fig. 12(d)] is patterned and etched using RIE. Next, as shown in Fig. 12(e), the oxide layer is etched with the poly masks for etching 15-μm trenches. Again, the poly layer is patterned and etched, and the oxide layer is etched for etching 8-μm trenches [Fig. 12(f)]. Then, the front via is patterned and etched 200-μm depth by deep dry etching [Fig. 12(g)]. After finishing via etching, the first mask layer of oxide was etched, and then the silicon trenches of 7.0 μm [as shown in Fig. 12(h)]. Then, the second mask layer of oxide is etched, and also the silicon trenches of 8.0 μm [Fig. 12(i)]. To this point, we have completed the fluid trenches and front via etching. The oxide layer as the hard-masks guarantees the accuracy of the geometry patterning and etching. Also, it guarantees that no patterning occurs in the deep trenches and through via and that no photoresist is trapped in the through via. Otherwise, the trapped photoresist will destroy the high-temperature furnace in the subsequent

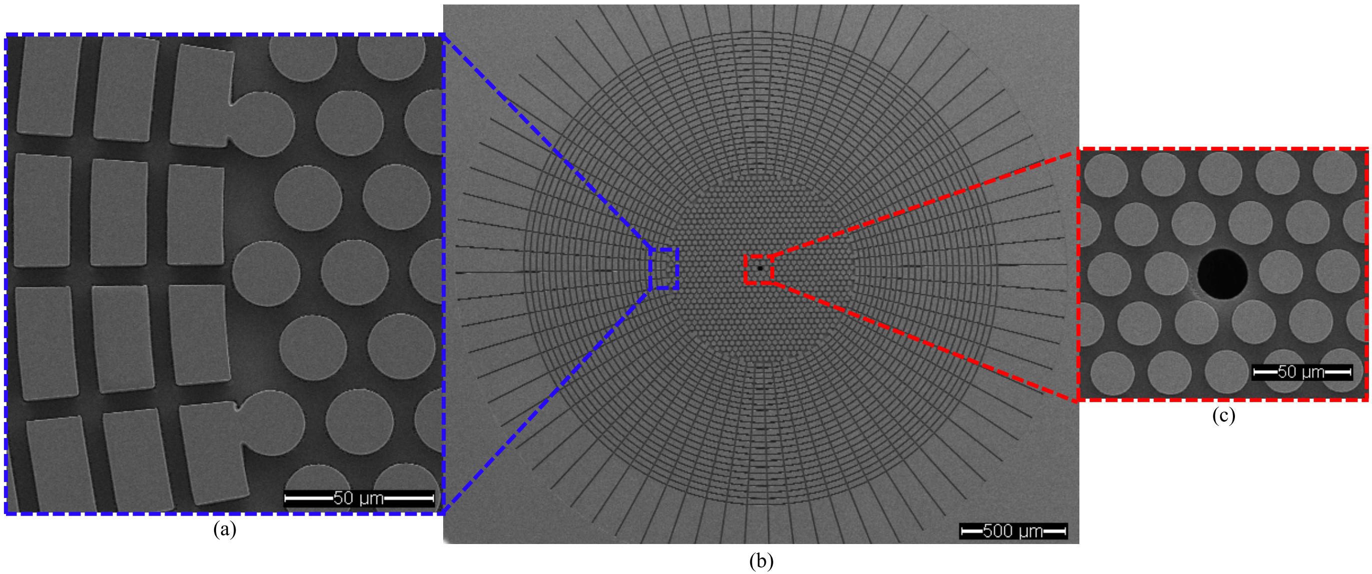

Fig. 13. SEM micrograph of the fluidic trenches in the substrate. (a) Fan-shaped hybrid trenches at the periphery. (b) Substrate of the vented CMUT with trenches. (c) Micropillar array at the center.

TABLE I
PARAMETERS OF THE VENTED CMUTs

Parameter	Value		
Plate radius (µm)		1500	
Plate thickness (µm)		50.5	
Gap height (µm)		1.01	
Oxide thickness (µm)		0.93	
Trench height (µm)	0	7.6	14.3

process. Then, all the poly layer and oxide layer are etched away using the DRIE and buffered HF solution. As shown in Fig. 12(j), another oxide layer of 1.0 μm is thermally grown as an insulating layer to prevent a short-circuit. The processed wafer is then bonded to a silicon-on-insulation (SOI) wafer [as shown in Fig. 12(k)] using direct fusion bonding techniques. After fusion bonding, the handling and buried oxide layers of the SOI wafer are removed by 30% KOH solution and buffered HF, respectively. A 300-nm-thick layer of aluminum is sputtered on the front and back of the bonded wafer to provide better electrical contact [Fig. 12(l)]. Then, the excess aluminum and silicon surrounding the CMUT element are patterned and etched away to reduce the parasitic capacitance [Fig. 12(m)]. Finally, the backside of the bonded wafers is patterned, and another 300 μm of Si is etched [as shown in Fig. 12(n)] to make the substrate vent through.

We could successfully fabricate devices that are very close to the design values. The deviation from the desired values for the gap height is less than 1%, and the maximum variation for the trench etching is less than 3%. The parameters are listed in Table I. Fig. 13 shows the SEM micrograph of the fluidic trenches in the substrate. Fig. 13(a) and (c) shows the micropillar array fluidic trenches with through via at the center, and the fan-shaped hybrid trenches at the periphery of the CMUT cell.

VI. CHARACTERIZATIONS

To verify the design theory, we have conducted impedance measurements and maximum sensitivity test then compared these results with finite element simulations. The comparison is made at the same percentage of dc bias of the pull-in voltage. Due to the residual stress in the SOI wafer, the fabricated plate bows up around 0.1 μm, which results in approximately a 10% higher pull-in voltage.

A. Impedance Measurements

The impedance data were obtained by an Impedance Analyzer (Agilent 4294A). Fig. 14 shows the measured impedance amplitude and phase of the vented CMUTs with 7.6- and 14.3-μm fluidic trenches. We can see that the impedance and pull-in voltage agree well with the simulations. The resonant frequency decreases as the trench height increases, because of the reduced stiffening effect of the squeeze film. The measured pull-in voltages are close to 54 V that also well match the simulations.

B. Maximum Displacement Sensitivity

The maximum displacement sensitivities were measured by Laser Doppler Vibrometer (LDV, Polytec OFV 2700 and OFV 511). As shown in Fig. 15, the displacement sensitivities for the vented CMUTs with different dc biases matched the FEM simulation results very well. The sensitivities of the vented CMUTs improve significantly by increasing the dc bias. However, the resonant frequency would shift to a lower frequency, which is caused by the so-called electrostatic spring softening effect. However, we can offset this effect by increasing the stiffening effect of the squeeze film. The BW is widened significantly from 6.0% to 8.1% when increasing the trench height.

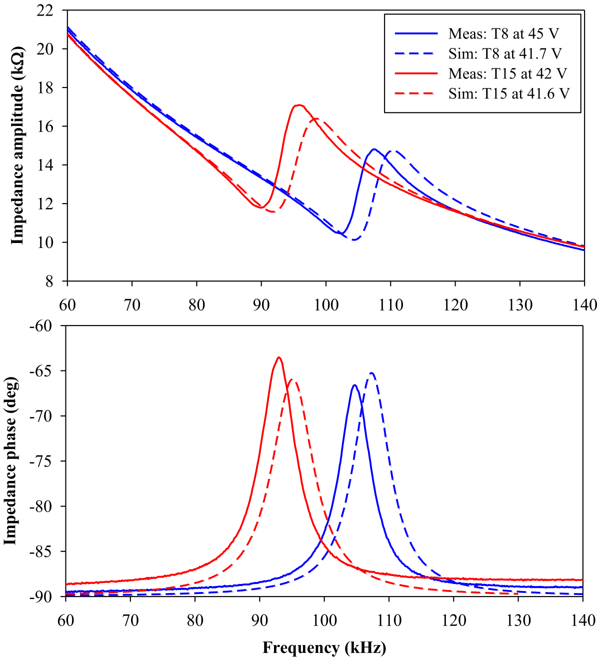

Fig. 14. Measured impedance of vented CMUTs with 7.6- and 14.3-μm fluidic trenches and comparison with FEM simulations. T8 is the CMUT with 7.6-μm trenches, and T15 is the CMUT with 14.3-μm trenches.

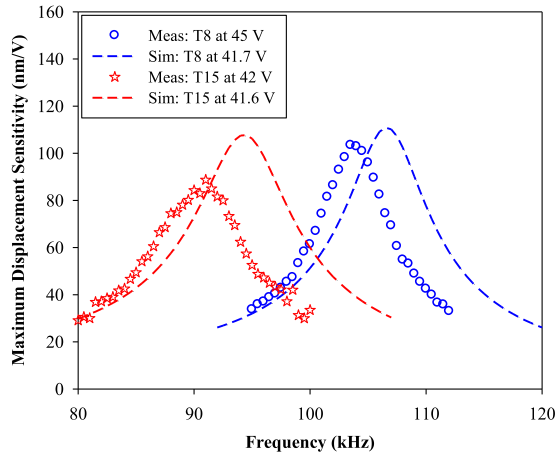

Fig. 15. Measured maximum displacement sensitivity of vented CMUTs with 7.6- and 14.3-μm trenches and comparison with FEM simulations. T8 is the CMUT with 7.6-μm trenches, and T15 is the CMUT with 14.3-μm trenches.

C. Minimum Detectable Pressure

The mechanical noise floor contributed by the medium damping R_m is equal to the noise force of R_m divided by the transducer area, and derived as follows:

$$P_{\text{in,min}} = \frac{\sqrt{4k_B \text{TR}_m}}{A_{\text{plate}}}. \tag{12}$$

Similarly, the equivalent noise contributed from the squeeze damping R_{sq} can be calculated. Therefore, the MDP $P_{\text{in,min}}$ in receive mode is associated with the noise contribution of the medium damping R_m and the squeeze film damping R_{sq}.

TABLE II
CHARACTERISTICS OF THE VENTED CMUTS

Type	DC Bias (%)	Resonant Frequency (kHz)	Bandwidth (%)	MDP (μPa/√Hz)
	0.8	175.9	0.89	2.20
T0	0.9	176.9	0.92	2.08
	0.95	178.2	0.97	2.18
	0.8	104.2	5.99	4.77
T8	0.9	102.4	6.41	5.41
	0.95	99.2	7.36	5.71
	0.8	92	8.12	4.88
T15	0.9	85.9	9.13	4.99
	0.95	81.8	10.2	5.28

T0 is the CMUT without trenches, T8 is the CMUT with 7.6 μm trenches, and T15 is the CMUT with 14.3 μm trenches.

The total equivalent noise can be given by

$$P_{\text{in,min}} = \frac{\sqrt{4k_B T (R_m + R_{\text{sq}})}}{A_{\text{plate}}}. \tag{13}$$

Based on the measured impedance, the MDP of the fabricated vented CMUTs is 4.77 μPa/$\sqrt{}$Hz with a 6.24-kHz BW for the vented CMUT with 7.6-μm fluidic trenches at the dc bias of 80% of the pull-in voltage while the MDP is 4.88 μPa/$\sqrt{}$Hz with a 7.48-kHz BW for the vented CMUT with 14.3 μm. These values well match the simulation results. Table II presents the characteristics of the fabricated vented CMUTs. The FBW can be easily controlled from 0.89% up to 10.2% by adjusting the trench height and dc bias.

VII. CONCLUSION

We have developed a novel method to increase the BW of airborne CMUTs, in which a gaseous squeeze film is used as a damping mechanism. By optimizing fluidic trenches with various heights, the behavior of the stiffening effect versus the damping mechanism of the squeeze film can be controlled. The stiffening effect also lowers the pull-in voltage and improves sensitivity. The sensitivity–BW product remains constant when increasing the trench height to widen the BW. Finally, the various CMUTs with different trench heights were fabricated on the same wafer using a multiple hard-mask microfabrication process. The measured impedance and maximum displacement sensitivity agreed with theory and FEM simulations. The FBW can be easily controlled from 0.89% up to 8.1% by only adjusting the trench height. The pull-in voltage was lowered to less than 54 V, which is 3.2 times decrease over the previous design. Meanwhile, we also obtain the noise equivalent pressure as lower to 4.88 μPa/$\sqrt{}$Hz with 7.48-kHz-wide BW, which makes the vented CMUTs capable of detecting weak signals for applications in biomedical and thermoacoustic imaging, as well as in nondestructive testing and ultrasonic flow metering.

ACKNOWLEDGMENT

The authors would like to acknowledge the support of the Stanford Nanofabrication Facility, Stanford, CA, USA, during the fabrication.

References

[1] K. K. Park and B. T. Khuri-Yakub, "3-D airborne ultrasound synthetic aperture imaging based on capacitive micromachined ultrasonic transducers," *Ultrasonics*, vol. 53, no. 7, pp. 1355–1362, Apr. 2013.

[2] S. Olcum, M. N. Senlik, and A. Atalar, "Optimization of the gain-bandwidth product of capacitive micromachined ultrasonic transducers," *IEEE Trans. Ultrason., Ferroelectr., Freq. Control*, vol. 52, no. 12, pp. 2211–2219, Dec. 2005.

[3] X. Zhang, F. Y. Yamaner, O. Adelegan, and Ö. Oralkan, "Design of high-frequency broadband CMUT arrays," in *Proc. IEEE Int. Ultrason. Symp. (IUS)*, Taipei, Taiwan, Oct. 2015, pp. 1–4.

[4] A. Unlugedik, A. Atalar, and H. Köymen, "Designing an efficient wide bandwidth single cell CMUT for airborne applications using nonlinear effects," in *Proc. IEEE Int. Ultrason. Symp.*, Prague, Czech Republic, Jul. 2013, pp. 1416–1419.

[5] A. Unlugedik, A. S. Taşdelen, A. Atalar, and H. Köymen, "Designing transmitting CMUT cells for airborne applications," *IEEE Trans. Ultrason., Ferroelectr., Freq. Control*, vol. 61, no. 11, pp. 1899–1910, Nov. 2014.

[6] M. Kupnik, M.-C. Ho, S. Vaithilingam, and B. T. Khuri-Yakub, "CMUTs for air coupled ultrasound with improved bandwidth," in *Proc. IEEE Int. Ultrason. Symp.*, Orlando, FL, USA, Oct. 2011, pp. 592–595.

[7] C. Bayram, S. Olcum, M. N. Senlik, and A. Atalar, "Bandwidth improvement in a cMUT array with mixed sized elements," in *Proc. IEEE Int. Ultrason. Symp.*, Rotterdam, The Netherlands, Sep. 2005, pp. 1956–1959.

[8] N. Apte, K. K. Park, A. Nikoozadeh, and B. T. Khuri-Yakub, "Bandwidth and sensitivity optimization in CMUTs for airborne applications," in *Proc. IEEE Int. Ultrason. Symp.*, Chicago, IL, USA, Sep. 2014, pp. 166–169.

[9] N. Apte, K. K. Park, and B. T. Khuri-Yakub, "Experimental evaluation of CMUTs with vented cavities under varying pressure," in *Proc. IEEE Int. Ultrason. Symp.*, Prague, Czech Republic, Jul. 2013, pp. 1724–1727.

[10] B. Ma, C. Chang, H. K. Oğuz, K. Firouzi, and B. T. Khuri-Yakub, "Multi-parameter optimization of vented CMUTs for airborne applications," in *Proc. IEEE Int. Ultrason. Symp.*, Washington, DC, USA, Sep. 2017, pp. 1–4.

[11] H. A. C. Tilmans, "Equivalent circuit representation of electromechanical transducers: I. Lumped-parameter systems," *J. Micromech. Microeng.*, vol. 6, no. 1, pp. 157–176, 1996.

[12] I. Ladabaum, X. Jin, H. T. Soh, A. Atalar, and B. T. Khuri-Yakub, "Surface micromachined capacitive ultrasonic transducers," *IEEE Trans. Ultrason., Ferroelectr., Freq. Control*, vol. 45, no. 3, pp. 678–690, May 1998.

[13] W. P. Mason, *Electromechanical Transducers and Wave Filters*. Princeton, NJ, USA: Van Nostand, 1942.

[14] A. Lohfink and P.-C. Eccardt, "Linear and nonlinear equivalent circuit modeling of CMUTs," *IEEE Trans. Ultrason., Ferroelectr., Freq. Control*, vol. 52, no. 12, pp. 2163–2172, Dec. 2005.

[15] A. Nikoozadeh, "Intracardiac ultrasound imaging using capacitive micromachined ultrasonic transducer (CMUT) arrays," Ph.D. dissertation, Dept. Elect. Eng., Stanford Univ., Stanford, CA, USA, 2010.

[16] S. D. Senturia, *Microsystem Design*. Boston, MA, USA: Kluwer, 2002, pp. 249–259.

[17] M. Kupnik, I. O. Wygant, and B. T. Khuri-Yakub, "Finite element analysis of stress stiffening effects in CMUTs," in *Proc. IEEE Ultrason. Symp.*, Beijing, China, Nov. 2008, pp. 487–490.

[18] J.-F. Li and J.-C. Pascal, "The influence of microphone vents on measurements of acoustic intensity and impedance," *J. Acoust. Soc. Amer.*, vol. 99, no. 2, pp. 969–978, Feb. 1996.

[19] P. R. Scheeper, A. G. H. van der Donk, W. Olthuis, and P. Bergveld, "A review of silicon microphones," *Sens. Actuators A, Phys.*, vol. 44, no. 1, pp. 1–11, Jul. 1994.

[20] M. Bao and H. Yang, "Squeeze film air damping in MEMS," *Sens. Actuators A, Phys.*, vol. 136, no. 1, pp. 3–27, 2007.

[21] D. Homentcovschi and R. N. Miles, "Modeling of viscous damping of perforated planar microstructures. Applications in acoustics," *J. Acoust. Soc. Amer.*, vol. 116, no. 5, pp. 2939–2947, Jul. 2004.

[22] D. Homentcovschi and R. N. Miles, "Viscous damping of perforated planar micromechanical structures," *Sens. Actuators A, Phys.*, vol. 119, no. 2, pp. 544–552, 2005.

[23] S. S. Mohite, H. Kesari, V. R. Sonti, and R. Pratap, "Analytical solutions for the stiffness and damping coefficients of squeeze films in MEMS devices with perforated back plates," *J. Micromech. Microeng.*, vol. 15, no. 11, pp. 2083–2092, Nov. 2005.

[24] W. S. Griffin, H. H. Richardson, and S. Yamanami, "A study of fluid squeeze-film damping," *J. Basic Eng.*, vol. 88, no. 2, pp. 451–456, 1966.

[25] J.-H. Meng, X.-X. Zhang, and X.-D. Wang, "Multi-objective and multi-parameter optimization of a thermoelectric generator module," *Energy*, vol. 71, pp. 367–376, Jul. 2014.

[26] A. S. Erguri, Y. Huang, X. Zhuang, Ö. Oralkan, G. G. Yarahoglu, and B. T. Khuri-Yakub, "Capacitive micromachined ultrasonic transducers: Fabrication technology," *IEEE Trans. Ultrason., Ferroelectr., Freq. Control*, vol. 52, no. 12, pp. 2242–2258, Dec. 2005.

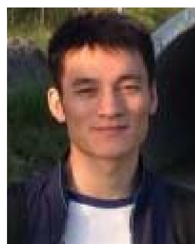

Bo Ma (GS'17) received the B.S. and M.S. degrees in electrical engineering from Jilin University, Changchun, China, in 2008 and 2010, respectively, and the Ph.D. degree in mechanical engineering from Tsinghua University, Beijing, China, in 2016.

He is currently a Postdoctoral Researcher with Stanford University, Stanford, CA, USA, working on the design and fabrication of airborne capacitive micromachined ultrasonic transducers (CMUTs). His current research interests include micromachined ultrasonic transducers, MEMS devices and systems integration, and micro/nanofabrication technology.

Kamyar Firouzi (M'16) received the M.S. degree in mechanical engineering from University College London (UCL), London, U.K., in 2010, and the Ph.D. degree in mechanical engineering from Stanford University, Stanford, CA, USA, in 2016. His Ph.D. dissertation was on the localization of objects in chaotic and reverberant enclosures, based on which he developed a Lamb-wave multi-touch ultrasonic touchscreen system.

He has worked on numerous problems in ultrasound/MEMS technologies, including the modeling and designing of ultrasonic transducers, photoacoustics, microbubbles, wave propagation, and numerical methods. His current research interests include transcranial ultrasound, ultrasound neuromodulation, ultrasonic flow measurement, and ultrasound signal processing and inverse problems.

Kevin Brenner received the B.S., M.S., and Ph.D. degrees in electrical engineering from the Georgia Institute of Technology, Atlanta, GA, USA, in 2007, 2009, and 2013, respectively.

He was the founder of a nanoelectronics device startup and has been awarded small business (SBIR) grants from the National Science Foundation, USA, Missile Defense Agency, and U.S. Air Force. He is currently a Postdoctoral Researcher with Stanford University, Stanford, CA, USA, working in the area of experimental device physics, and supported by an Intelligence Community Fellowship.

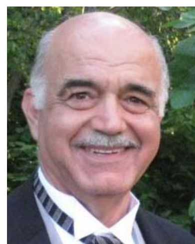

Butrus (Pierre) T. Khuri-Yakub (S'70–M'76–SM'87–F'95–LF'18) received the B.S. degree in electrical engineering from the American University of Beirut, Beirut, Lebanon, in 1970, the M.S. degree in electrical engineering from Dartmouth College, Hanover, NH, USA, in 1972, and the Ph.D. degree in electrical engineering from Stanford University, Stanford, CA, USA, in 1975.

He is currently a Professor of electrical engineering with Stanford University. He has authored over 552 publications and holds 93 U.S. and internationally issued patents. His current research interests include medical ultrasound imaging and therapy, ultrasound neurostimulation, chemical/biological sensors, gas flow and energy flow sensing, micromachined ultrasonic transducers, and ultrasonic fluid ejectors.

Dr. Khuri-Yakub was awarded the medal of the City of Bordeaux in 1983 for his contributions to nondestructive evaluation, the Distinguished Advisor Award of the School of Engineering at Stanford University in 1987, the Distinguished Lecturer Award of the IEEE UFFC Society in 1999, the Stanford University Outstanding Inventor Award in 2004, the Distinguished Alumnus Award of the School of Engineering of the American University of Beirut in 2005, the Stanford Biodesign Certificate of Appreciation for commitment to educate, mentor, and inspire Biodesign Fellows in 2011, and the 2011 IEEE Rayleigh Award.